JOURNAL OF
REINFORCED
PLASTICS &
COMPOSITES

Original Article

Journal of Reinforced Plastics and Composites
2014, Vol. 33(15) 1375–1387

DOI: 10.1177/0731684414529832
jrp.sagepub.com
SAGE

An investigation into the performance of composite hat stringers incorporating nanocomposites using a multiscale framework

Zeaid Hasan, Aditi Chattopadhyay and Yingtao Liu

Abstract

In this paper, an effort has been made to investigate the incorporation of carbon nanotubes in structural composites in order to improve damage characteristics, such as delamination. The nanocomposite material is introduced in the damage-prone regions of complex aerospace stiffener sections; the methodology proposed is an alternative to traditional approaches used to suppress delamination in composites, such as the use of metallic fittings. Numerical simulations are conducted using a multiscale modeling framework. The effective properties of the nancomposites are computed using a micromechanics-based approach and the results are compared with those obtained using a Kalman filter algorithm. The information is then used to analyze the structural response of a hat stringer using detailed finite element models. The stringer is analyzed under different loading conditions and varying levels of defects in the structure. Results obtained indicate that the use of nanocomposites improves the structural performance by improving the initial failure load. It is anticipated that the use of carbon nanotubes during the manufacturing process will help delay the onset of initial damage and damage growth, which can ultimately lead to a more robust structural design with enhanced performance against unique composite failure modes.

Keywords

Nanocomposites, interlaminar failure, delamination, fracture, hat stringers

Introduction

Laminated composites have been widely used in a variety of applications; particularly where weight-critical structures are required to have high in-plane stiffness and strength. Several researchers have investigated the analysis of composite materials and their use in aircraft structures under different loading conditions using experimental, numerical and analytical methods.[1–14] However, the potential use of these composites has been compromised by weak out-of-plane properties, especially delamination resistance. With considerable effort towards solving the problem of delamination in fiber-reinforced laminates, it is found that the factors most contributing to the delamination are the weak fiber/ matrix interface and the brittle nature of the matrix resin. In structures made out of composites, delamination may be suppressed by changing the architecture of the reinforcement through the introduction of thickness-reinforcing elements (e.g. 3D textiles, stitching).[15,16] However, these modifications to the micro-structure of the composite do not change the inherent interface and matrix properties. The weak interface and low matrix toughness should be addressed on the fundamental level of the composite structure that defines these properties (i.e. below the micro-structure, on the nano level). This can be done through surface modification of the fibers, and toughening of

School for Engineering of Matter, Transport and Energy, Arizona State University, AZ, USA

Corresponding author:
Zeaid Hasan, School for Engineering of Matter, Transport and Energy, Arizona State University, Tempe, AZ 85004, USA.
Email: zeadnws@hotmail.com

the matrix by embedding CNTs into the matrix material forming nanocomposites.

Since the nanocomposite is on a macro continuum scale, while the individual phases can range from the continuum scale down to the nanometer scale, challenges arise while attempting to model the nanocomposites analytically or numerically. Modeling of nano materials must follow a systematic procedure, which aids in transitioning material properties from one scale to another. At the macro scale, continuum modeling methods, such as finite element (FE) modeling, are utilized to design composite structures based on loading conditions.

Recently, it has been reported that the addition of carbon nanotubes (CNTs) in the polymer matrix can increase the toughness of the matrix and improve the interface properties of CNT-composites.[17,18] Furthermore, multiscale reinforcement containing fibers together with CNTs in the matrix or on the surface of the fibers can increase delamination resistance of fiber-reinforced composites.[19–29] In those cases, delamination resistance is increased due to different mechanisms of interaction between the propagating cracks with nanotubes such as crack deflection, CNT pullout, crack tip deformation, and so on.

In light of the information above, it can be observed that the use of nanocomposites at the structural level may render a solution to the delamination problem; therefore, the authors were motivated to initiate such investigation. The objectives of this paper are to understand the effects of using nanocomposites in structural level composite joints, and their ability to improve the unique composite failure modes. In this study, the authors focus on delaminations that exist around the tow filler of a composite hat stringer as well as the interface between the skin and stringer. Different loading conditions were taken into consideration, such as pull-off and combined (pull-off/axial) loading. The virtual crack closure technique is used to determine the initial damage, which will be used as the dependent variable in this study to compare the results and determine the percent improvement from using CNTs.

The paper is organized as follows. First, a description of the multiscale analysis is presented that provides the effective mechanical properties of the nanocomposites at the different length scales. An estimation approach based on adopting the Kalman filter framework is also presented as a means to provide a more optimized approach in determining the effective properties, which relies on input from experiments in combination with mathematical relations provided from the micromechanics approach. Second, validation of the numerical analysis that is based on FE modeling is presented, where results are compared with available experimental data in the literature. Third, the analysis of the hat stringer is discussed and the structural responses are evaluated and compared for different CNT weight percentages and different loading conditions. Finally, some concluding remarks are presented based on the research results.

Effective mechanical properties of nanocomposites

Micromechanics approach

Modeling of nanocomposites requires a systematic approach, taking into account the various length scales (nano, micro, meso and macro) and associated constitutive behavior and the transfer of relevant information across these length scales. For such a multiscale analysis framework to be useful in practical applications, it is also important to ensure computational efficiency while maintaining accuracy. The work presented here is based on a systematic approach that allows for the transition from a single or multi-walled CNT to a composite lamina. First, the effective properties of the CNT are calculated. Next, the effective properties of a nanocomposite made of epoxy with embedded effective nanotubes are calculated; these properties are then used as matrix properties to calculate the effective properties of a composite lamina. These properties are then utilized in a structural level analysis to assess the structural integrity using FE analysis.

In this study, both the composite cylinder[30] and the Mori-Tanaka[31] methods will be used in conjunction to determine the effective elastic properties. The composite cylinder method is utilized to determine the effective properties of the CNT. This method uses both energy equivalency and direct averaging to determine the properties.[30] Multi-layered composite cylinder assemblage could be taken into account in this method, to simulate multi-wall CNTs with interfacial layers as shown in Figure 1. To acquire the effective elastic properties of aligned fiber composites using the composite cylinders method, the volume averaged strain energies of both the composite cylinder assemblage, W, and of the effective homogeneous cylinder, W^{eff}, are obtained from the volume average of the strain energy, and are set equal to one another providing a set of boundary value problems to be solved. The solution to these problems enabled the calculation of the effective material in-plane bulk modulus, axial Young's modulus, the axial stiffness component, the axial shear modulus, and the in-plane shear modulus.

The effective CNT properties are used as inputs in the Mori–Tanaka method to calculate the effective mechanical properties of the nanocomposite (epoxy with embedded effective nanotubes). The effective stiffness tensor is obtained by embedding a solid cylinder

that has the effective CNT properties in the unknown effective composite, and is obtained as[32]

$$C = \left(v_m C_m \tilde{L}_m + \sum_{l=1}^{P} v_l C_l \tilde{L}_l \right) \left(v_m I + + \sum_{l=1}^{P} v_p \tilde{L}_p \right)^{-1} \quad (1)$$

$$\tilde{L}_l = \left[I + S L_m^{-1} (L_l - L_m) \right]^{-1} \quad (2)$$

where C represents the effective stiffness tensor, L is the concentration tensor, v is the volume fraction, S is the eshelby tensor, and I is the identity tensor. The concentration tensor (L) relates the average strain in the effective cylinder to the average strain of the matrix and is perturbed by some amount to account for interactions between inclusions. S is obtained for cylindrical inclusions embedded in the matrix. Once the effective properties of the nanocomposite are obtained, they are used as the new matrix material to formulate the nanocomposite lamina. Both unidirectional and woven composites can be considered using this approach.

In order to analytically model the nanocomposite lamina, the stiffness matrix for an infinitesimal slice must be obtained. This is done by adding stiffness matrices of the constituents as follows[33]

$$K_{ij}(x, y) = \sum_{I} v_I(x, y) \overline{Q}_{ij}^{I}(x, y), \quad i, j = 1 - 6 \quad (3)$$

where $\overline{Q}_{ij}^{I}$ is the transformed stiffness matrix (to the global frame) of the I^{th} element. Superscript I refers to either the fill strand (F), the warp strand (W) when considering woven composites, or the matrix (M). To calculate the global stiffness matrix $K_{global}(x, y)$, the local matrix $K_{ij}(x, y)$ is evaluated for a small slice over x and y directions in an averaged manner as follows

$$K(y) = 1/a \int_0^a K(x) \mathrm{d}x \quad (4)$$

$$K_{gobal} = 1/a \int_0^a K(y) \mathrm{d}y \quad (5)$$

where a represents the strand or fiber width. Equations (4) and (5) are used to calculate the effective properties of the nanocomposite lamina.

Estimation approach

An alternative approach in determining the effective mechanical properties of the nanocomposites is investigated in this study. It is based on an estimation framework that utilizes the Kalman filter algorithm. The process depends on user-defined mathematical models of the phenomenon under study, and measurements acquired by a practical experiment or application to optimally estimate certain parameters. The motivation in presenting the following method is to validate the results obtained from the micromechanics approach, and to provide an alternative method to determine the effective properties. The Kalman filter utilizes both the micromechanics methods and results from FE models to estimate the material properties.

Consider a detailed FE model of a nanocomposite with hollow cylindrical CNTs, such as the one shown in Figure 2. The displacements obtained from this model

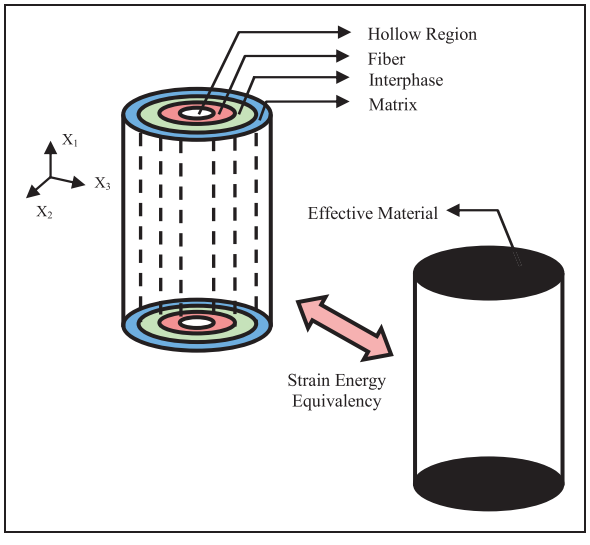

Figure 1. Graphical representation of the multi-layered composite cylinder method.

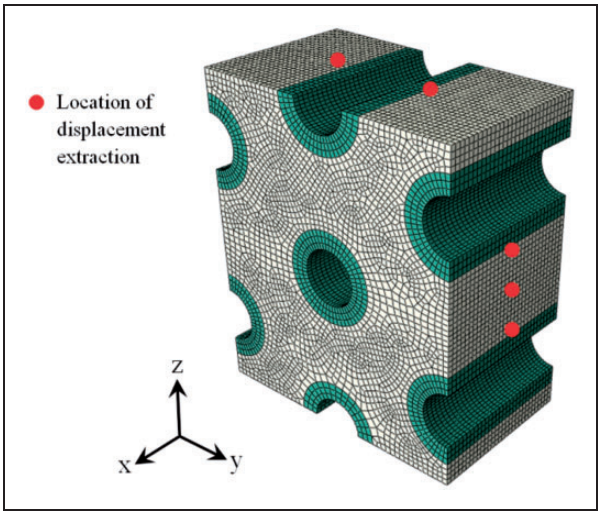

Figure 2. Detailed FE model of the nanocomposite represented volume element (RVE).

as a result of an applied load can be considered as a measured value. This simulated measurement is synonymous to having a strain gauge attached to the specimen at different locations, which are represented by the red dots in Figure 2. Now consider a homogenous solid FE model, as the one shown in Figure 3, with properties acquired by the analytical micromechanics solution. This homogenous model is considered a mathematical representation of an actual nanocomposite where at an applied load (equal to that applied to the detail FE model) a certain displacement is achieved. A displacement function is generated by varying the properties of the homogenous model and applying the same load every time. This displacement function acts as the mathematical model required for the Kalman filter. The Kalman filter utilizes the measured displacement (analogous to experiment) and the calculated displacement (homogeneous model) to optimally estimate the material parameters. Figure 4 shows a flow chart of the general Kalman filter structure followed in this study.

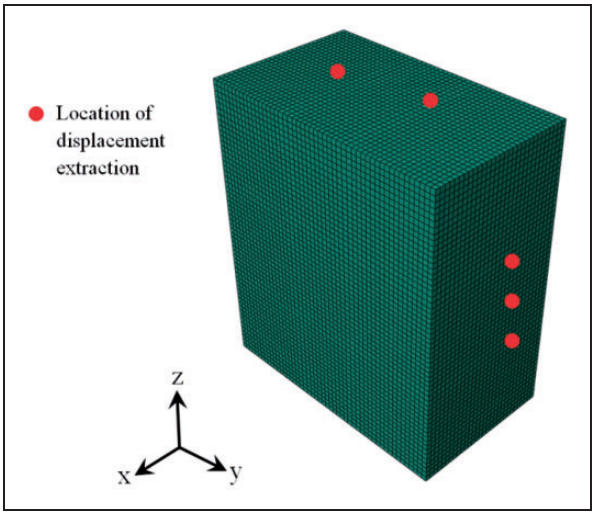

Figure 3. Homogenous FE model of the nanocomposite RVE.

Finite element model construction and validation

This section discusses the FE models and the method used to analyze the structure. In order to validate both the modeling techniques and the method of analysis, the results are first compared with available experimental data.[6] The computer software CATIA is used to create the CAD geometry, and the commercial software Abaqus is used for the FE analysis. Particular attention is paid to issues such as boundary conditions, mesh refinement, and contact behaviors. Selecting the proper fastener modeling technique is also a key issue. The modeling techniques that are considered in the analysis utilize solid continuum elements (C3D8I) for the composite parts as well as the metallic fixtures and fasteners. An Abaqus connector modeling routine (star-fastener) is used to represent the fasteners in

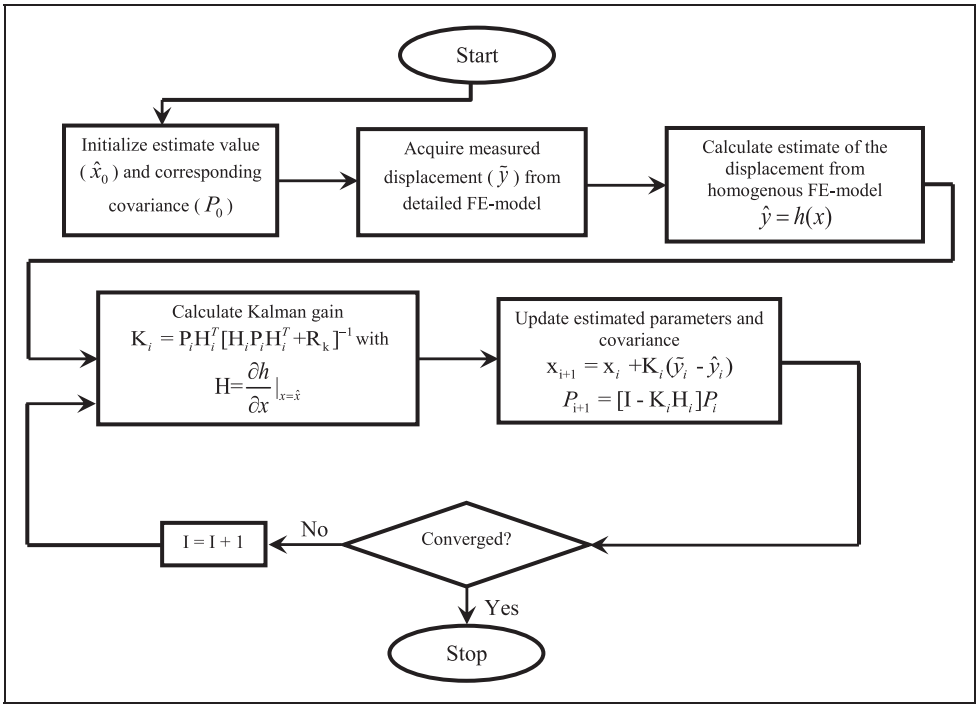

Figure 4. Estimation approach flow chart.

the model. These connectors use multi-point constraints (MPCs) to fix nodes on each surface in a fastener stack-up with respect to a central reference point that lies on the fastener axis centerline. Separate "axial" and "shear" connector definitions are used at each fastener location to provide both in-plane and thru-thickness constraints to the surfaces in the fastener stack-up.

The virtual crack closure technique is used in this analysis to detect initial damage. When the stress intensity reaches the critical strain energy release rate, the central pair of nodes is released. A damage index is defined as follows[12]

$$\lambda = \frac{G_{equiv}}{G_{equivC}} = \left(\frac{G_I}{G_{IC}}\right)^m + \left(\frac{G_{II}}{G_{IIC}}\right)^n + \left(\frac{G_{III}}{G_{IIIC}}\right)^o \quad (6)$$

where G_I, G_{II}, and G_{III} are the strain energy release rates for modes *I*, *II*, and *III* fractures, respectively; G_{Ic}, G_{IIc}, and G_{IIIc} are the allowed toughness for modes *I*, *II*, and *III* fractures respectively; and superscripts *m*, *n*, and *o* are equal to 1 in this study. When this damage index reaches a unit value, it implies that a node has been released and initial damage has been detected. In order to utilize the virtual crack closure technique, an initial flaw must be embedded in the model. Usually, the flaw is inserted in locations where delamination is most likely to occur. In order to correlate to the available experimental data, a 0.75 inch $\times$0.75 inch flaw is considered and inserted between the tow filler and the web midway along the stringer span, as shown in Figure 5, since delamination was observed to initiate from that location.[6] It is noteworthy to mention that preload is applied to all the fasteners in the model and resin toughness values are used in the analysis to predict the initial damage.[34] It is noted that the failure is usually dominated by mode I fracture, and the contribution of modes II and III is not significant. Figure 6 shows the correlation between the FE model and the experimental data. Note that the correlation was done to the initial damage load and not the final failure load. A total of nine specimens were tested that were 7 inches long and had varying widths (1, 2, 3 inches).[6] It can be observed that the predicted initial damage from the FEM is within 10% of the results obtained from the test data. Note that the initial damage predicted by the models is lower, indicting that the models provide a more conservative estimate. This correlation provided the authors with confidence in both the analysis method and modeling techniques, and therefore is used for the remaining analysis.

Hat stringer analysis with embedded CNTs

Delamination is considered to be one of the primary forms of failure in laminated composite structures, especially when there is no reinforcement in the thickness direction. In order to develop composite structures that are more tolerant, and resistant to interlaminar failure, it is necessary to understand how delamination develops and how it can affect the performance. Residual thermal stresses, matrix-curing shrinkage, and manufacturing defects are all factors that determine how damage will initiate and grow in a composite structure. The high stress gradients that occur in specific hotspots in the structure, such as the tow filler and the skin/stringer bondlines (that exist in composite hat stringers), promote damage initiation and may cause a significant loss of structural integrity. The use of nanocomposite in such critical locations may alleviate such problems and help improve the overall structural performance.

After having correlated to available experimental data, confidence was gained with the modeling techniques used in terms of fastener idealization, mesh density, elements types, etc. The next step is to create a comparatively larger and detailed model with the same modeling methods that incorporate the use of fine grid mesh, especially in the area of interest, to be

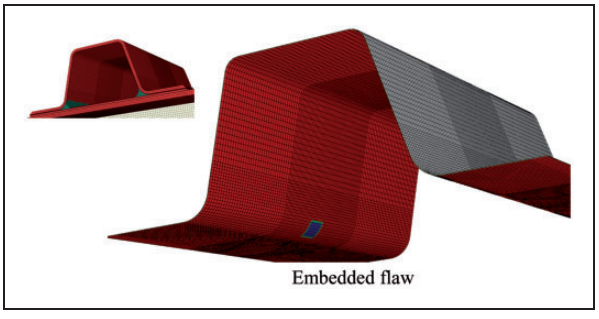

Figure 5. Embedded flaw used in the model.

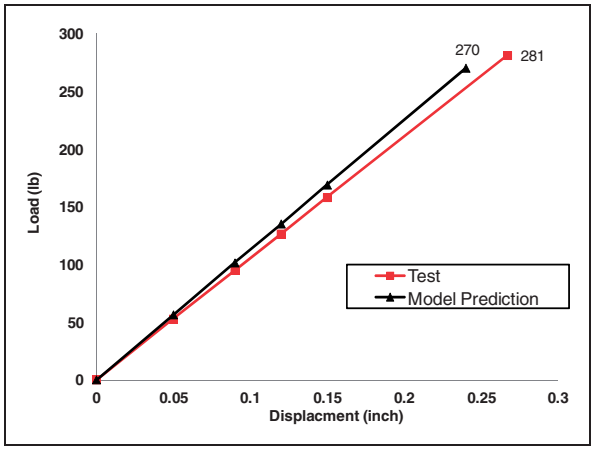

Figure 6. Correlation between the FE model and test.

able to accurately capture the joint behavior under the critical loading conditions. In order to better understand the structural performance, several different damage scenarios and loading conditions are considered. Table 1 summarizes the different flaws and loading condition combinations. A schematic diagram of the different flaw types is shown in Figure 7. A comparison between using pure adhesive and one with 1, 3, and 5 weight percent CNT is considered. Modes I, II, and III fracture toughness for adhesive is used in the analysis. It was found that the fracture toughness values increase significantly for adhesive that incorporates CNTs in their mixture[35–37] which motivated the authors to consider that as an alternative to overcome some of the structural weaknesses in composite joints.

Table 1. Summary of the different flaws and loading condition combinations used in the analysis.

Flaw type	Loading condition	Tow material	Case
Flaw 1	Pull-off	Fabric	1
		Adhesive	2
	Pull-off + Axial	Fabric	3
		Adhesive	4
Flaw 2	Pull-off	Fabric	5
		Adhesive	6
	Pull-off + Axial	Fabric	7
		Adhesive	8
Flaw 3	Pull-off	Fabric	9
		Adhesive	10
	Pull-off + Axial	Fabric	11
		Adhesive	12

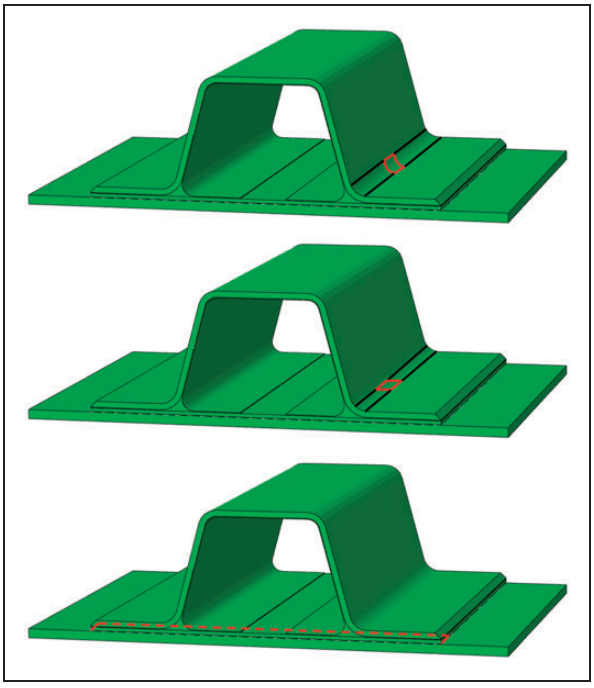

Figure 7. Schematic of the stringer configuration with the different flaws considered in the analysis.

Numerical results

Mechanical properties of nanocomposites

Much research has been conducted for the purpose of predicting the properties of nanocomposites that include CNTs embedded in polymer matrix.[35–39] However, the study of composites consisting of CNTs, fibers, and a matrix material has not received the same attention. The goal of the results presented in this section is to provide insight on the effect of adding CNTs to the mechanical properties at the structural level, and to compare the results obtained from the estimation framework with that from the micromechanics framework at the CNT/epoxy level. The effect of changing the CNT volume fraction on the elastic composite properties is shown. Table 2 shows the elastic and geometric properties of the CNT used in the analysis. Figure 8 presents the variation of the nanocomposite unidirectional lamina mechanical properties as a function of CNT volume fraction. The results show an increase in the axial and lateral elastic modules as the CNT volume fraction increases. The same behavior can be seen in the shear modules. Poisson's ratio, on the other hand, decreases as the volume fraction increases.

A comparison between the results obtained from the estimation framework and the micromechanics for the matrix/CNT nanocomposite is shown in Figure 9. It can be observed that the properties estimated by the Kalman filter are comparable to those calculated by the micromechanics approach for Young's modulus and shear modulus. Based on the approach and results presented, the Kalman filter can be easily utilized as a first method of system identification for estimating material properties of nanocomposites using strain measurements. The results also highlight the validity of the micromechanics results, which were derived earlier to calculate effective properties of nanocomposites since the estimates relied on set expressions and yielded acceptable results.

Table 2. Mechanical and geometrical properties of CNTs.

Variable	Value
Young's modulus	159.5 Msi
Poisson's ratio	0.14
Wall thickness	13.26 e^{-9} inch

Failure analysis of composite stringers incorporating CNTs

A schematic diagram of the hat stinger model is shown in Figure 10. As mentioned earlier, different flaw types are considered in this study as well as two types of designs regarding the composite stringer; one that uses adhesive to fill the tow region and another that uses fabric. The reason for using these designs is the fact that both are typically utilized in the manufacturing of such stringers. Moreover, different composite laminate designs (a design that use CNTs embedded

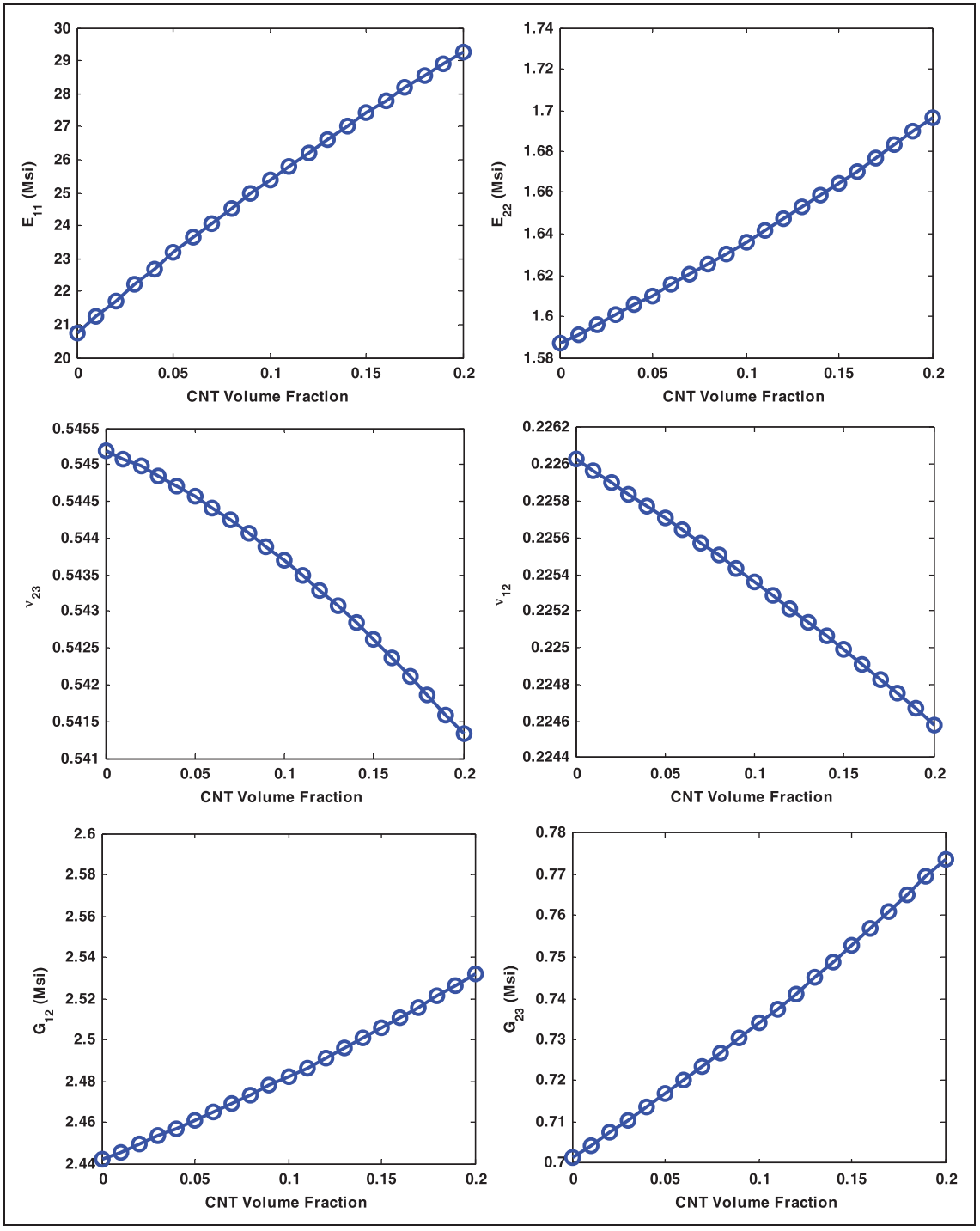

Figure 8. Effective properties of the nanocomposite lamina as a function of CNT volume fraction.

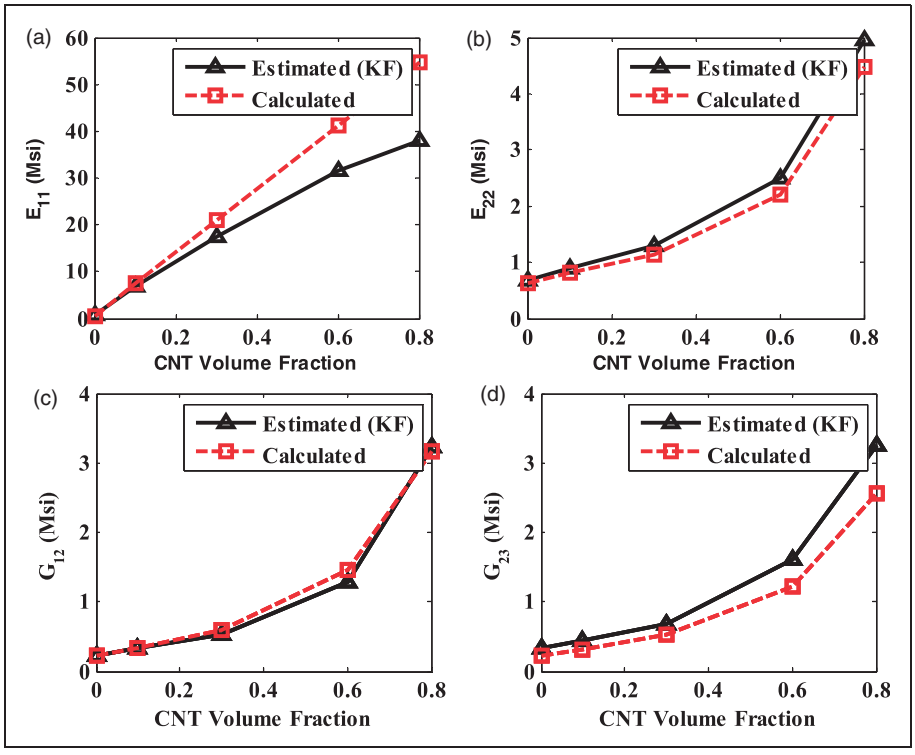

Figure 9. Effective properties of the nanocomposite as a function of CNT volume fraction—estimated and calculated.

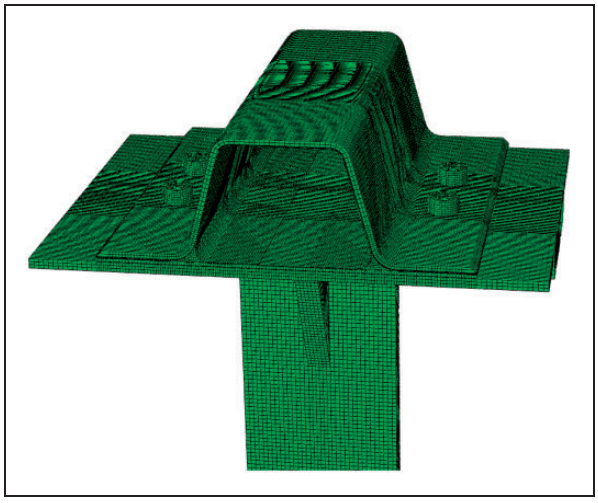

Figure 10. 3D mesh of the hat stringer.

in the matrix and others that use pure epoxy for the matrix material) are also studied. The loading conditions considered were pull-off and combined axial/pull-off. It is important to note that the value of the failure load depends on the location where the flaw is embedded in the structure. The peak running load exists midway; hence, both flaw types 1 and 2 are embedded in the hat stringer in that location, whereas flaw type 3 is inserted at the stringer termination between the stringer base and skin interface.

Figures 11–13 show the initial failure load by applying a pure pull-off load for the three different flaw types. Note that four different configurations regarding the use of CNT in the structure were considered, and are summarized in Table 3. Figure 11 represents the pull-off failure load of the structure that incorporates a flaw of type 1. The general trend that was observed for both types of tow materials (fabric and adhesive) was the increase in failure load with increase in CNT weight fraction due to the added through thickness capability. It is also noticeable from the figure that for all values of CNT weight fractions, the failure load for the adhesive tow is considerably larger than that for the fabric tow. In addition, when examining the adhesive and fabric tow results, the failure load is higher when both the tow material and the composite lamina contain CNTs. Flaw type 1 was noted to be mode I dominant, which relies on the angle opening of the radius where the pull-off load tends to open the radius creating high energy release rates. Therefore, the use of CNTs was shown to give additional through thickness capability, preventing or delaying such event from occurring. Figure 12 represents the pull-off failure load of the structure that incorporates a flaw of type 2. In this case, the failure load increased with the increase in CNT weight percentage for both types of tow materials (fabric and adhesive). It can also be observed that the failure load for the adhesive tow is significantly larger than that for the fabric tow. By considering only the

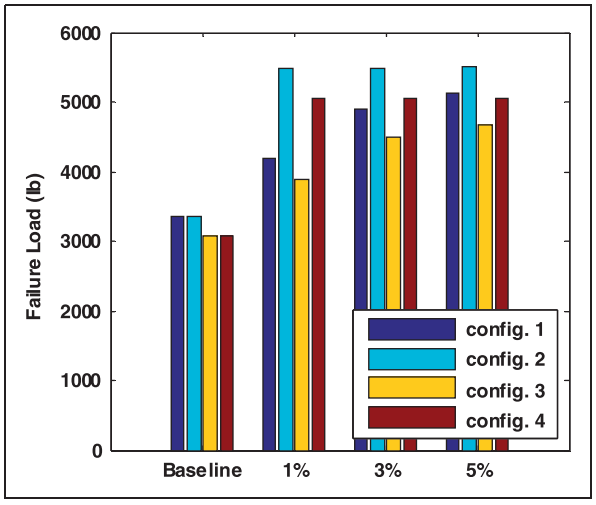

Figure 11. Pull-off failure load for flaw 1 considering different configurations.

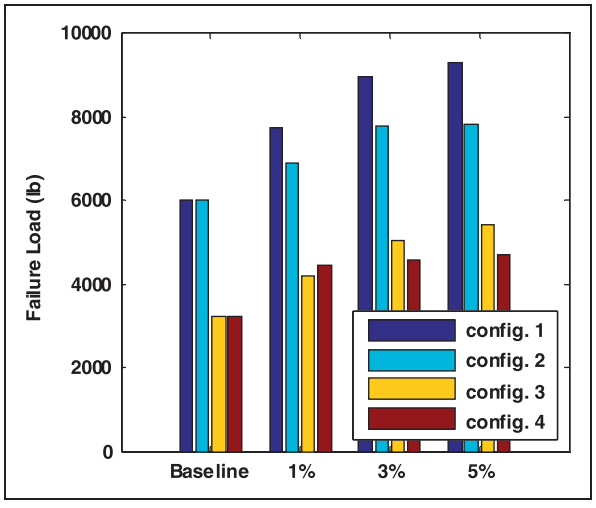

Figure 12. Pull-off failure load for flaw 2 considering different configurations.

adhesive tow results, the failure load was higher when only the adhesive tow contains CNTs; therefore, there is no additional gain from using CNTs in the composite lamina. On the other hand, when considering the fabric tow configuration, the failure load is higher when both the tow material and composite contain CNTs. Flaw type 2 was also found to be mode I dominant under pull-off loading, and the use of CNTs was shown to give additional through thickness capability preventing or delaying such events from occurring. It can also be noted that the failure load is much higher for this flaw type compared to the previous case, which means that the structure has more capability of sustaining additional load with the inclusion of this flaw type under

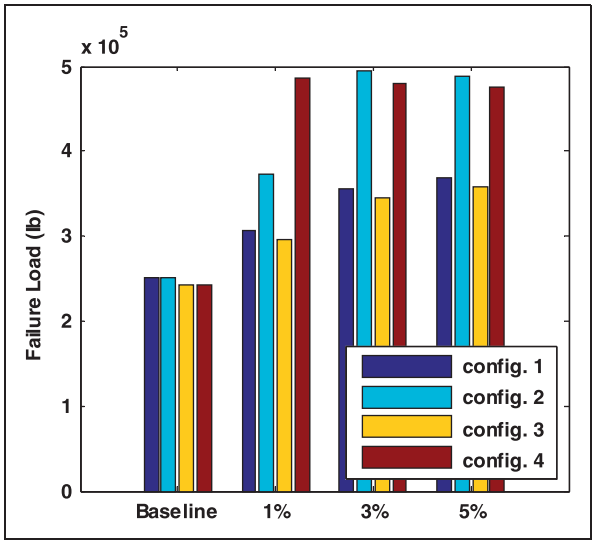

Figure 13. Pull-off failure load for flaw 3 considering different configurations.

Table 3. Different configurations considered in the analysis.

Configuration	Use of CNT
1	**Adhesive Tow** (CNT was used in the adhesive layer surrounding the tow filler and the tow filler itself. CNT was also used in the adhesive layer that exists between the skin and stringer interface)
2	**Adhesive Tow** (CNT was used in the adhesive layer surrounding the tow filler and the tow filler itself. CNT was also used in the adhesive layer that exists between the skin and stringer interface. In addition, CNT was used in the composite laminates of the stringer and skin)
3	**Fabric Tow** (CNT was used in the adhesive layer surrounding the tow filler and the tow filler itself. CNT was also used in the adhesive layer that exists between the skin and stringer interface)
4	**Fabric Tow** (CNT was used in the adhesive layer surrounding the tow filler and the tow filler itself. CNT was also used in the adhesive layer that exists between the skin and stringer interface. In addition, CNT was used in the composite laminates of the stringer and skin)

pull-off loading. That is an important observation when designing the structure from the damage-tolerance perspective. Figure 13 represents the pull-off failure load of the structure that incorporates a flaw of type 3. As in the previous two cases, the failure load increases with increase in CNT weight percentage; however, for the

fabric tow, the failure load increases up until 5% CNT by weight where it drops slightly. When examining the adhesive tow results, the failure load is higher when both the adhesive and the composite lamina contain CNTs and the same statement holds for the fabric tow. Flaw type 3 was found to have a mode mix of both I and II under pull-off loading, and the use of CNT was shown to give additional through thickness capability in this case as well.

The combined loading effect is addressed next. Both the axial and pull-off loads are applied simultaneously; therefore, the cause of initial damage is not distinguishable. Figure 14 shows a schematic diagram of the loading condition. Figures 15–17 show results for the same weight fractions, flaw types, and tow design as shown previously for the pure pull-off case. However, they differ in the loading condition that was applied; in this case, combined axial/pull-off was applied to the structure. In these figures, only the axial load at which initial failure occurred was reported. Figure 15 represents results from considering a flaw of type 1. The dominating trend that can be observed was that the axial failure load increased as the CNT weight fraction increased. Also, the axial failure load for the fabric tow was always larger than that of the adhesive tow for all cases. There is, however, substantial gain in failure load if the CNTs were used in both adhesive and composite lamina. Figure 16 represents the axial failure load of the structure that incorporates a flaw of type 2 under combined axial/pull-off load. It can be

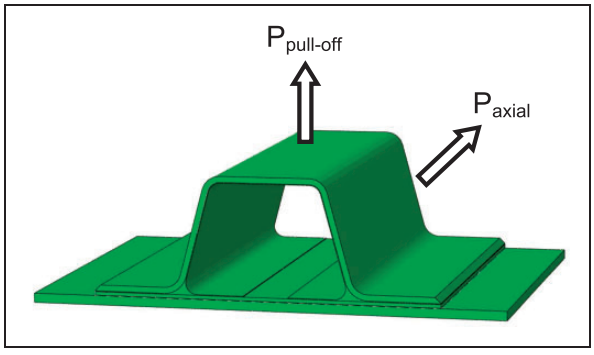

Figure 14. Schematic diagram of the combined loading condition.

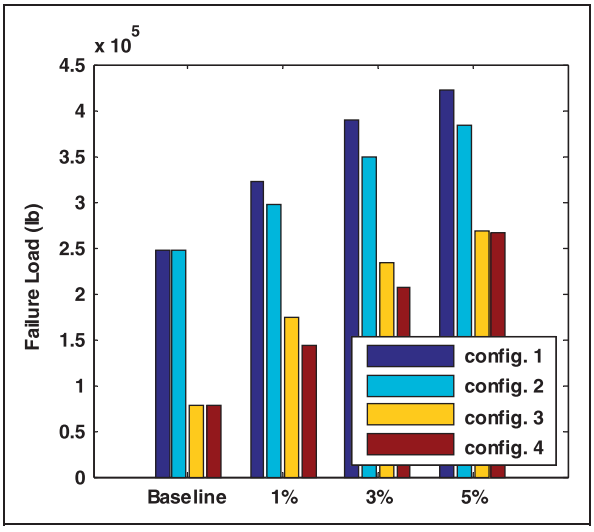

Figure 16. Axial failure load for flaw 2 by applying a combined axial/pull-off load for different configurations.

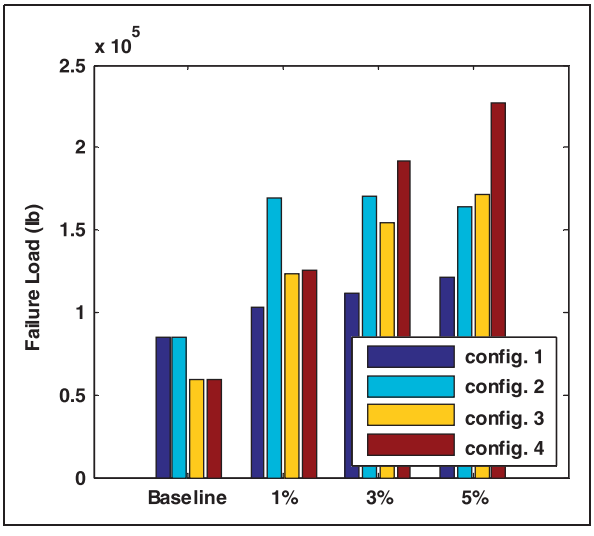

Figure 15. Axial failure load for flaw 1 by applying a combined axial/pull-off load for different configurations.

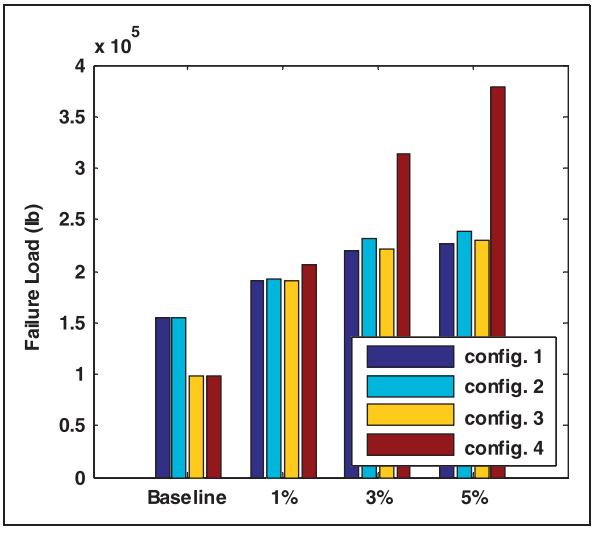

Figure 17. Axial failure load for flaw 3 by applying a combined axial/pull-off load for different configurations.

observed for both types of tow materials (fabric and adhesive) that as the CNT weight fraction increases, the failure load increases. It is also clear from the figure that for all values of CNT weight fractions, the failure load for the adhesive tow is larger than that for the fabric tow. Moreover, the failure load is higher when the CNTs are only used in the adhesive. This may be attributed to the location of the flaw and its interaction with the surrounding structure under the applied axial load. Figure 17 represents the axial failure load of the structure that incorporates a flaw of type 3. For both types of tow material, it can be observed that as the CNT weight fraction increases, the failure load increases. It is also obvious from the figure that for all values of CNT weight fractions, the axial failure load for the fabric tow was larger than that for the adhesive tow. In addition, the failure load for cases of CNTs being present in the adhesive and composite lamina was larger than when only having it used in the adhesive. Note that a substantial increase in failure load is obtained for having CNTs weight of 3% and above for the design that incorporates the use of fabric tows, and CNT used in the adhesive and composite lamina.

Figures 18–20 show the failure load that occurred due to the pull-off loading from the combined loading case. Figure 18 shows the results for type 1 flaw; the dominating trend is that the failure load increases as the CNT weight fraction increases, and the failure load is higher for the fabric tow for all weight fractions. In addition, there is substantial gain in pull-off failure load if the CNTs are used in the adhesive and composite lamina. Figure 19 shows the initial pull-off failure load for flaw of type 2. The failure load is observed to increase as the CNT weight fraction increases. It is noted that the failure load remains constant whether the CNT was used in the adhesive only or in the composite lamina as well; therefore, having them in the adhesive only would reduce cost and manufacturing complexity while sustaining similar failure load. Figure 20 represents the pull-off failure load of the structure that incorporates a flaw of type 3. It is noted from the figure that the pull-off failure load varies with configuration. A substantial increase in failure load is obtained by having CNT weight of 1% and above for configuration 4. It should be noted from the

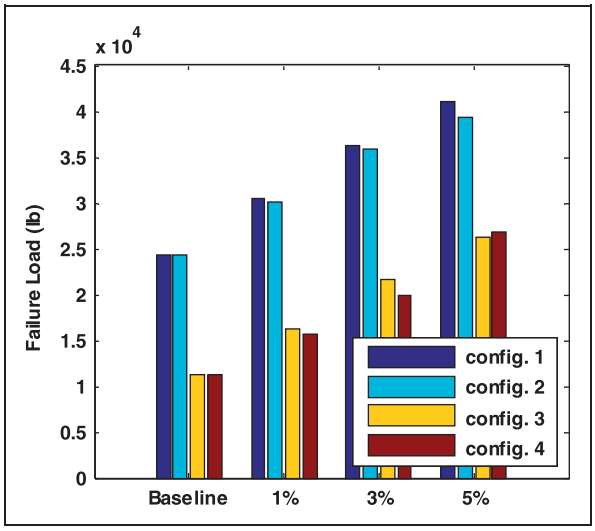

Figure 19. Pull-off failure load for flaw 2 by applying a combined axial/pull-off load for different configurations.

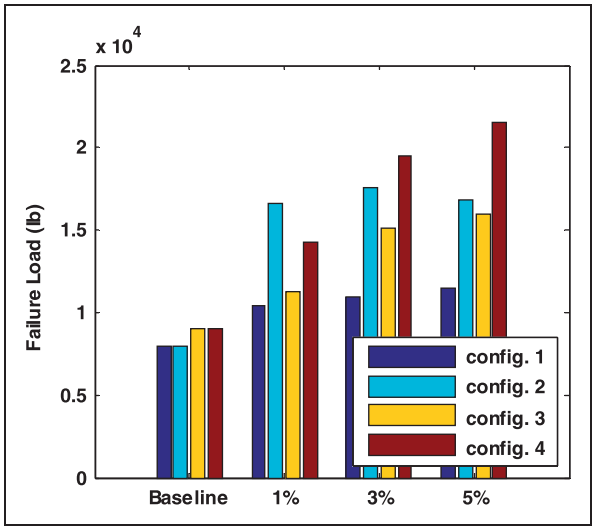

Figure 18. Pull-off failure load for flaw 1 by applying a combined axial/pull-off load for different configurations.

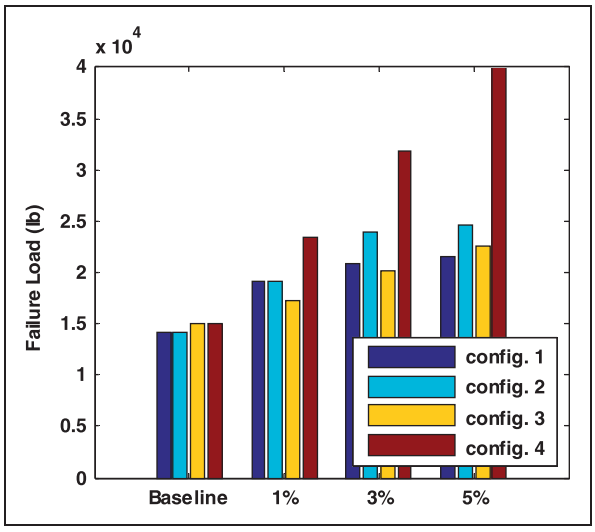

Figure 20. Pull-off failure load for flaw 3 by applying a combined axial/pull-off load for different configurations.

previous results that the axial failure load is much higher than the failure that occurs from pull-off. Moreover, combined loading consideration is an important part in the analysis and design process of such structures; since, as was observed, the failure loads could be under or overestimated providing a structure that might be less conservative or overly designed, respectively.

From the results presented in this section, it can be concluded that an aerospace structure (such as stringers) subjected to pull-off loading the use of CNTs in specific hot spot locations, such as the tow-stringer web interface or the bondline location between the skin and stringer, can prevent or delay the onset of delamination.

Conclusion

The present study focused on the benefits of using nanocomposites in structural level components that are typically used in aerospace applications. An example of such structure was a typical hat stringer. A multiscale approach was used to determine the effective properties of the nanocomposite at different length scales. These effective properties were used in the FE models. An alternative approach in determining the effective mechanical properties was also presented; it was based on an estimation method using the Kalman filter. The results were compared with those obtained from the micromechanics approach. It was found that the Kalman filter can be easily utilized as a first method of system identification for estimating material properties of nanocomposites using strain measurements. The results also highlight the validity of the micromechanics results.

A detailed model was constructed of the Hat stinger bonded to a skin in order to assess the use of nanocomposites in structural level components to improve some of the weak spots in such structures. The virtual crack closure technique was adopted in order to determine the initial damage of the structure, defined as the initial load drop in the load displacement curve. Different configuration, flaw types, and loading conditions were considered in this study. By comparing the initial failure loads it was shown that using CNTs in the manufacturing process of such stringers might improve the overall performance up to 35%. It was also concluded that when considering a structure that experiences pull-off loading, the use of CNTs in hotspot locations, such as the tow-stringer web interface or the bondline location between the skin and stringer interface, the delamiantion that occurs in those locations can be prevented or delayed thereby providing a much more robust structural design.

Funding

The authors are grateful for the support of NAVAIR grant, sponsored by Integrated Systems Solutions (Grant number: W911NF-12-1-0353).

Conflict of interest

None declared.

Acknowledgement

Dr Nam Phan is the program manager.

References

1. Ostergaard M, Ibbotson A, Le Roux O, et al. Virtual testing of aircraft structures. *Aeronaut J* 2011; 1: 83–103.
2. Martin R. Local fracture mechanics analysis of stringer pull-off and delamination in a post-buckled compression panel. *J Appl Compos Mater* 1996; 3: 249–264.
3. Krueger R, Cvitkovich M, O'brien K, et al. Testing and analysis of composite skin/stringer debonding under multi-axial loading. *J Compos Mater* 2000; 34: 1263–1300.
4. Winzen A. *Simulation of stringer stiffened CFRP panels in consideration of skin-stringer separation*. Master Thesis, Aachen University of Applied Sciences, Department of Aerospace Technology, Germany, 2006.
5. Hoyt D, Ward S and Minguet P. Strength and fatigue life modeling of bonded joints in composite structure. *J Compos Technol Res* 2002; 24: 188–208.
6. Li JA, Brien TK and Rousseau CQ. Test and analysis of composite hat stringer pull-off test specimens. *J Am Helicopter Soc* 1997; 42: 350–357.
7. Cope RD and Pipes RB. Design of the composite spar–wing skin joint. *J Compos* 1982; 13: 47–53.
8. Rispler AR, Steven GP and Tong L. Failure analysis of composite T-joints including inserts. *J Reinf Plastics Compos* 1997; 16: 1642–1658.
9. Kumari S and Sinha PK. Finite element analysis of wing T-joints. *J Reinf Plastics Compos* 2002; 21: 1561–1585.
10. Zimmermann K, Zenkert D and Siemetzki M. Testing and analysis of ultra thick Composites. *J Compos Part B* 2010; 41: 326–336.
11. Helenon F, Wisnom MR, Hallett SR, et al. Numerical investigation into failure of laminated composite T-piece specimens under tensile loading. *J Compos Part A: Appl Sci Manuf* 2012; 43: 1017–1027.
12. Panigrahi SK and Pradhan B. Delamination damage analyses of FRP composite spar wing skin joints with modified elliptical adhesive load coupler profile. *J Appl Compos Mater* 2008; 15: 189–205.
13. Panigrahi SK and Pradhan B. Development of load coupler profiles of spar wingskin joints with improved performance for integral structural construction of aircraft wings. *J Reinf Plastics Compos* 2009; 28: 657–673.
14. Chen J, Ravey E, Hallett S, et al. Prediction of delamination in braided composite T-piece specimens. *J Compos Sci Technol* 2009; 69: 2363–2367.

15. Tong L, Mouritz A and Bannister M. *3D fibre reinforced polymer composites*, 1st ed. Boston: Elsevier, 2002, pp.1–12.
16. Dransfield K, Jain L and Mai Y. On the effects of stitching in CFRPs-I. mode I delamination toughness. *J Compos Sci Technol* 1998; 58: 815–827.
17. Thostenson E, Ren Z and Chou T-W. Advances in the science and technology of carbon nanotubes and their composites: a review. *J Compos Sci Technol* 2001; 61: 1899–1912.
18. Abdala M, Dean D, Adibempe D, et al. The effect of interfacial chemistry on molecular mobility and morphology of multiwalled carbon nanotubes epoxy nanocomposite. *J Polymer* 2007; 48: 5662–5670.
19. Bekyarova E, Thostenson ET, Yu A, et al. Multiscale carbon nanotube–carbon fiber reinforcement for advanced epoxy composites. *Langmuir* 2007; 23: 3970–3974.
20. Garcia EJ, Hart AJ and Wardle BL. Long carbon nanotubes grown on the surface of fibers for hybrid composites. *J AIAA* 2008; 46: 1405–1412.
21. Garcia EJ, Wardle BL, Hart AJ, et al. Fabrication and multifunctional properties of a hybrid laminate with aligned carbon nanotubes grown in situ. *J Compos Sci Technol* 2008; 68: 2034–2041.
22. Godara A, Warrier A, Mezzo L, et al. Influence of carbon nanotube reinforcement on the mechanical behavior of carbon fiber/epoxy composites. In: *SAMPE 2008, Europe international conference and forum*, Paris, 8–11 September 2008.
23. Godara A, Warrier A, Mezzo L, et al. Influence of carbon nanotube reinforcement on the processing and the mechanical behaviour of carbon fiber/epoxy composites. *J Carbon* 2008; 47: 2914–2923.
24. Wichmann MHG, Sumfleth J, Gojny FH, et al. Glass-fibre-reinforced composites with enhanced mechanical and electrical properties – benefits and limitations of a nanoparticle modified matrix. *J Eng Fract Mech* 2006; 73: 2346–2359.
25. Qian H, Bismarck A, Greenhalgh ES, et al. Hierarchical composites reinforced with carbon nanotube grafted fibers: the potential assessed at the single fiber level. *J Chem Mater* 2008; 20: 1862–1869.
26. Qu LT, Zhao Y and Dai LM. Carbon microfibers sheathed with aligned carbon nanotubes: towards multidimensional, multicomponent, and multifunctional nanomaterials. *J Small* 2006; 2: 1052–1059.
27. Romhány G and Szebényi G. Interlaminar crack propagation in MWCNT/ reinforced hybrid composites. *eXPRESS Polymer Lett* 2009; 3: 145–151.
28. Tan P, Tong L and Sun X. Effective properties for plain weave composites through thickness reinforced with carbon nanotube forests. *J Compos Struct* 2008; 84: 1–10.
29. Thostenson ET, Li WZ, Wang DZ, et al. Carbon nanotube/carbon fiber hybrid multiscale composites. *J Appl Phys* 2002; 91: 6034–6037.
30. Christensen R and Lo K. Solutions for effective shear properties in three phase sphere and cylinder models. *J Mech Phys Solids* 1979; 27: 315–330.
31. Mori T and Tanaka K. Average stress in matrix and average elastic energy of materials with misfitting inclusions. *Acta Metallurg* 1973; 21: 571–574.
32. Gary DS and Dimitris CL. Micromechanical analysis of the effective elastic properties of carbon nanotube reinforced composites. *J Mech Mater* 2006; 38: 884–907.
33. Scida D, Aboura Z, Benzeggagh ML, et al. A micromechanics model for 3D elasticity and failure of woven-fiber composite materials. *Journal Composites and Science and Technology* 1999; 59: 505–517.
34. Li J and Sen J. Analysis of frame-to-skin joint pull-off tests and prediction of the delamination failure. In: *Proceedings of the 42nd structures, structural dynamics, and materials (SDM) conference*, Seattle, Washington, AIAA-2001-1484, 16–19 April 2001.
35. Kumar JSP, Raghava G and Stanley AJ. Fracture toughness of multi walled carbon nano tubes modfied polymer composite in mode – I. *J Mater Sci Res* 2012; 1: 117–123.
36. Hsieh T, Kinloch A and Taylor A. The effect of carbon nanotubes on the fracture toughness and fatigue performance of a thermosetting epoxy polymer. *J Mater Sci* 2011; 46: 7525–7535.
37. Thakre P, Lagoudas D, Riddick J, et al. Investigation of the effect of single wall carbon nanotubes on interlaminar fracture toughness of woven carbon fiber–epoxy composites. *J Compos Mater* 2011; 0: 1–17.
38. Selmi A, Friebel C, Doghri I, et al. Prediction of the elastic properties of single walled carbon nanotube reinforced polymers: A comparative study of several micromechanical models. *J Compos Sci Technol* 2007; 67: 2071–2084.
39. Peeterbroeck S, Breugelmans L, Alexandre M, et al. The influence of the matrix polarity on the morphology and properties of ethylene vinyl acetate copolymers-carbon nanotube nanocomposites. *J Compos Sci Technol* 2007; 67: 1659–1665.